Stereo Camera Calibration with an Embedded Calibration Device and Scene Features

Xiameng Qin, Jiaolong Yang, Wei Liang, Mingtao Pei and Yunde Jia

Abstract— **In this paper, a new stereo camera calibration technique that can realize automatic strong calibration is proposed. In order to achieve online camera calibration, an object covered with chess-board patterns, called embedded calibration device, is placed inside the cavity of the stereo-vision system. We estimate the structural configuration of the embedded calibration device, i.e. the 3D positions of all the grid points on the device, to calibrate the cameras. Since the device is close to the stereo camera, the calibration results are usually not valid for the volume around the object in the scene. Therefore we present a correction approach combining the embedded calibration and scene features to make the calibration valid in the scene. Experimental results demonstrate that our system performs robust and accurate, and is very applicable in unmanned systems.**

I. INTRODUCTION

Camera calibration is a necessary step of stereovision to extract metric information from 2D images. Conventional camera calibration [1], [2], [15] has generally been done by a procedure whereby a 3D calibration device whose spatial geometry is designed or measured with very high-precision. The calibration device is placed in front of a camera, then the imaged positions of features on this device are used to estimate the camera parameters. Such calibration can determine exact camera parameters and recover the absolute scale of a scene owing to some explicit 3D information. The development of plane-based camera calibration [6], [9], [16] makes the calibration flexible and easy to use. The planar pattern is required to be shown at different orientations observed by the camera to be calibrated, and the images containing the planar patterns are used to estimate the camera parameters. The camera calibration technique based on 1-D object [7], [19], [22] is also significant in practice especially in multi-camera calibration problem [10]. The 1-D object rotates around a fixed point, or undergoes a special motion so that it can be observed in different orientations. This calibration approach would fail in the degenerate cases or critical motions, which have been investigated by Hammarstedt *et al* [11].

However, those techniques suffer from two problems. One problem is that the calibration procedure usually requires human interaction to position the calibration object and then to remove it after calibration. Moreover, calibration object must be observed from several different orientations to obtain accurate results. Another problem is that the calibration is only effective for the region around the position of calibration objects [17]. The further the scene is, the more instability the performance of the calibration would be.

In order to overcome the problem of human interaction and the degeneration of the calibration performance when the scene is away from the camera, Zhang [17] proposed an on-site stereo calibration method in which the calibration device is mounted on the vehicle. Nevertheless, one can only re-calibrate the vision system at intervals using this method. On the other hand, the spatial geometry of the calibration object must be designed with high-precision. Katayama [3] proposed a calibration method that uses a transparent calibration tool with affixed dot patterns of color filter material. This tool, installed in front of the camera, does not need to be reset or removed, so that it greatly simplifies the calibration process. This is an online automatic calibration technique, but the accuracy of this method is not comparable with the conventional methods because the calibration tool is located far away from the plane of focus.

Self-calibration is a kind of online auto-calibration method which has been explored intensively in last two decades [12], [21], [26]. These methods only make use of a number of image correspondences to estimate camera parameters. However, self-calibration processes are rather unstable even if they have been lead with caution [4]. In some cases, several calibration parameters (such as principal points) are assumed to be known [8], or an initial guess of the camera parameters should be provided [20].

In this paper, we propose a new stereo camera calibration technique with an embedded calibration device and scene features. An embedded calibration method is implemented with the calibration device hidden inside the cavity of the embedded calibration stereovision system. The system will not require human interaction to place and remove the calibration device. Considering that the embedded calibration is not valid for the volume around the scene because the distance from the scene to the cameras is farther than the distance between the calibration device and the cameras, we present an optimization approach to correct the embedded calibration results with scene features.

Fig. 1 shows the sketch of our embedded calibration stereovision system. The system consists of a stereo head, a half-mirror, an embedded calibration device, and a light source. The calibration device comprises three planes, and each plane is covered with a chess-board pattern. The light source will be turned on during calibration, and turned off after calibration. The half-mirror completely reflects the

Xiameng Qin, Jiaolong Yang, Wei Liang, Mingtao Pei and Yunde Jia are with Beijing Lab of Intelligent Information Technology, School of Computer Science, Beijing Institute of Technology, Beijing 100081, PR CHINA. {liangwei, peimt, jiayunde}@bit.edu.cn

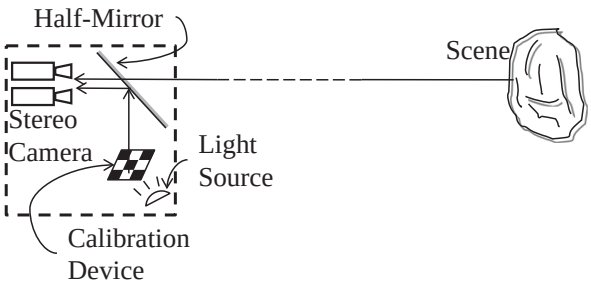

Fig. 1. The embedded calibration stereovision system.

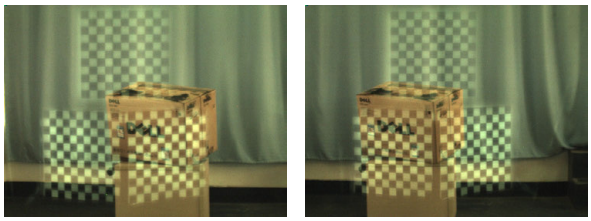

Fig. 2. An embedded calibration stereo pair.

calibration device to the stereo camera while it also allows the scene rays passing through itself and reaching the camera. It enables the stereo camera to simultaneously observe the scene and the calibration device to generate an embedded calibration stereo pair, as shown in Fig. 2. The detailed description of the embedded calibration stereovision system could be found in our previous work [14].

II. EMBEDDED CALIBRATION

The ideal pinhole camera model is applied in this paper to describe the stereo camera in our system. Let $\mathbf{X} = [X, Y, Z]^T$ and $\mathbf{x} = [x, y]^T$ be a 3D point in the world coordinate system and its corresponding 2D image point in the pixel coordinate system respectively. $\widetilde{\mathbf{X}} = [X, Y, Z, 1]^T$ and $\widetilde{\mathbf{x}} = [x, y, 1]^T$ denote their homogenous coordinates. Then the projective relation is given by

$$\widetilde{\mathbf{x}} \sim \mathbf{P}\widetilde{\mathbf{X}} = \mathbf{K}\begin{bmatrix}\mathbf{R} & \mathbf{t}\end{bmatrix}\widetilde{\mathbf{X}} = \begin{bmatrix}\alpha & \gamma & u_0 \\ 0 & \beta & v_0 \\ 0 & 0 & 1\end{bmatrix}\begin{bmatrix}\mathbf{R} & \mathbf{t}\end{bmatrix}\widetilde{\mathbf{X}}, \quad (1)$$

where $\mathbf{P}$ is the 3x4 projection matrix; $\mathbf{K}$ is the intrinsic camera matrix; α,β,γ,u_0,v_0 are the intrinsic parameters; $\mathbf{R}$ and $\mathbf{t}$ are extrinsic parameters defining the rotation and translation from the world coordinate system to the camera coordinate system. The symbol $\sim$ means equality up to a scale.

In our system, the three planes are fixed so the spatial relationships among the three planes, or furthermore the relative 3D positions of all the corner points on the three planes, could be used as a prior to achieve more robust calibration. Thus before calibration, the structural configuration of the calibration device should be estimated.

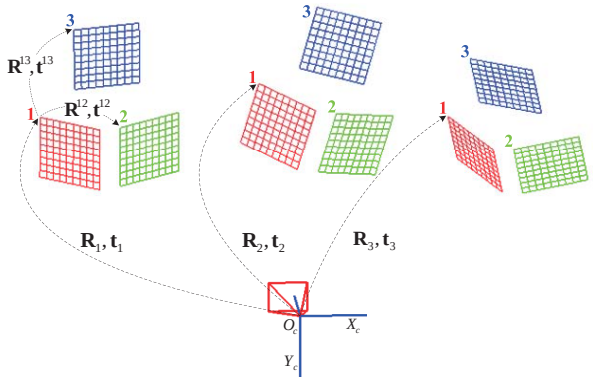

Fig. 3. Configuration estimation of the embedded calibration device. The device is moved n times in front of the camera. n equals 3 in this illustration whereas n is greater than 10 in practice to obtain better results.

A. Configuration Estimation of the Calibration Device

Let $\mathbf{R}^{12}$, $\mathbf{t}^{12}$ and $\mathbf{R}^{13}$, $\mathbf{t}^{13}$ be the rotation matrix and translation vector from the first plane to the second plane and third plane respectively. As illustrated in Fig. 3, the device is moved n times in front of a high resolution camera. (It should be clear that the camera used here is NOT the camera to be calibrated using our system. A higher resolution camera may guarantee finer structural computation results because of the better image quality.) Let $\mathbf{R}_i$, $\mathbf{t}_i$ $(0 < i < n)$ denote the transformation from the camera coordinate system to the i-th device coordinate system centered at the top-left grid point on the first plane. The initial closed-form solution of $\mathbf{R}^{12}$, $\mathbf{t}^{12}$, $\mathbf{R}^{13}$, $\mathbf{t}^{13}$ and each $\mathbf{R}_i$, $\mathbf{t}_i$ can be easily computed using the method in [16]. Then these parameters are refined by the maximum likelihood estimation minimizing the reprojection error given by the cost function

$$\sum_{i=1}^{n}\sum_{j=1}^{m}\left\|\mathbf{x}_{ij} - \hat{\mathbf{x}}_{ij}\left(\mathbf{K}, k_1, k_2, \mathbf{R}_i, \mathbf{t}_i, \mathbf{R}^{12}, \mathbf{t}^{12}, \mathbf{R}^{13}, \mathbf{t}^{13}, \mathbf{X}_j\right)\right\|^2, \quad (2)$$

where $\mathbf{x}_{ij}$ and $\hat{\mathbf{x}}_{ij}$ are the measured and predicted image point corresponding to the 3D point $\mathbf{X}_j$; k_1, k_2 are the distortion factors; m is the number of grid points on the device.

After configuration estimation, the coordinates of all the 3D corner points on the calibration device in the device coordinate system are known and can be used to calibrate other cameras.

B. Online Stereo Calibration

In the stereo calibration stage, image positions of the known 3D corner points projected on the image are extracted using Harris corner detector. An iteration process similar to [27] is applied to refine the positions of extracted grid points. Since the calibration patterns might be far away from the plane of focus, the image of calibration pattern would be blurred, resulting in difficulties with Harris corner localization. To alleviate this problem, we introduce the geometry constraint, such as collineation and intersection, among all the corner points to refine the coordinates of the

points in each iteration. The iteration will repeat until the root mean square (RMS), computed between the coordinates measured by the Harris corner detector and the coordinates predicted with the geometry constraint, is less than a predefined value ξ. Finally, the coordinates of all the grid points are accurately extracted by the above procedure and used in calibration.

Given correspondences between image points $\mathbf{x}_i$ and 3D point $\mathbf{X}_i$, we should find the 3x4 projection matrix $\mathbf{P}$ such that $\widetilde{\mathbf{x}}_i \sim \mathbf{P}\widetilde{\mathbf{X}}_i$ for all i. The linear estimation of $\mathbf{P}$ is found via Direct Linear Transform (DLT) [26] as the initial solution. Then a maximum likelihood estimation which can be solved with the LM method is used to minimize the reprojection error

$$\sum_{i=1}^{n} \left\| \mathbf{x}_i - \hat{\mathbf{x}}_i \left(\mathbf{P}, \mathbf{X}_i \right) \right\|^2. \tag{3}$$

Once the projection matrix $\mathbf{P}$ is estimated, the camera parameters $\mathbf{K}$, $\mathbf{R}$ and $\mathbf{t}$ can also be readily computed (by QR decomposition).

The left and right cameras are calibrated separately with the calibration device at the fixed position. Let $\mathbf{K}_L$, $\mathbf{R}_L$, $\mathbf{t}_L$ and $\mathbf{K}_R$, $\mathbf{R}_R$, $\mathbf{t}_R$ be the calibration matrices of the left and right camera from embedded calibration. Then the transformation from the left camera to the right camera would be

$$\begin{cases} \mathbf{R} = \mathbf{R}_R \mathbf{R}_L^{-1} \\ \mathbf{t} = -\mathbf{R}_R \mathbf{R}_L^{-1} \mathbf{t}_L + \mathbf{t}_R \end{cases}. \tag{4}$$

III. EMBEDDED CALIBRATION CORRECTION WITH SCENE FEATURES

Since the embedded calibration is only valid around the embedded calibration device, and the calibration performance degrades if the scene is away from this region, the embedded calibration results should be corrected such that they will be effective for the volume around the scene. In this paper, the feature points in the scene are extracted from the two images of the left and right camera and matched. The *epipolar constraint* [18], [26], which describes the constrain on the matched feature point pairs, is introduced to establish the correlation between the camera parameters (including the intrinsic parameters and extrinsic parameters) and the scene feature points, and correct the camera parameters.

The fundamental matrix $\mathbf{F}$ is the algebraic expression of epipolar geometry. Referring to the parameters of the left and right camera with subscripts L and R respectively, a pair of corresponding points $\mathbf{x}_L$ and $\mathbf{x}_R$ in the left image and right image satisfies the condition

$$\widetilde{\mathbf{x}}_R^T \mathbf{F} \widetilde{\mathbf{x}}_L = 0 \tag{5}$$

where $\widetilde{\mathbf{x}}_L$ and $\widetilde{\mathbf{x}}_R$ are the homogeneous coordinates of the corresponding points $\mathbf{x}_L$ and $\mathbf{x}_R$, and

$$\mathbf{F} = \mathbf{K}_R^{-T} \left[\mathbf{t} \right]_\times \mathbf{R} \mathbf{K}_L^{-1} \tag{6}$$

where $\mathbf{R}$ and $\mathbf{t}$ are the rotation matrix and translation vector from the left camera coordinate system to the right camera coordinate system, and $\left[\mathbf{t} \right]_\times$ is the skew-symmetric matrix of the vector $\mathbf{t}$.

Let $\widetilde{\mathbf{x}}_{L_i}$ and $\widetilde{\mathbf{x}}_{R_i}$ denote the homogeneous coordinates of a pair of corresponding points, the epipolar error can be given by

$$\epsilon_i = \frac{| \hat{\mathbf{l}}_{L_i}^T \widetilde{\mathbf{x}}_{L_i} |}{\sqrt{\hat{\mathbf{l}}_{L_i[1]} + \hat{\mathbf{l}}_{L_i[2]}}} + \frac{| \hat{\mathbf{l}}_{R_i}^T \widetilde{\mathbf{x}}_{R_i} |}{\sqrt{\hat{\mathbf{l}}_{R_i[1]} + \hat{\mathbf{l}}_{R_i[2]}}} \tag{7}$$

where $\hat{\mathbf{l}}_{p[q]}$ indicates the q-th component of vector $\hat{\mathbf{l}}_p$. The vectors

$$\hat{\mathbf{l}}_{L_i} \sim -\mathbf{K}_L^{-T} \mathbf{R}^T [\mathbf{t}]_\times \mathbf{K}_R^{-1} \mathbf{x}_{L_i} \tag{8}$$

and

$$\hat{\mathbf{l}}_{R_i} \sim \mathbf{K}_R^{-T} [\mathbf{t}]_\times \mathbf{R} \mathbf{K}_L^{-1} \mathbf{x}_{R_i} \tag{9}$$

are the directions of the epipolar lines computed by the corresponding point pairs and the camera matrices. Thus, the objective function of the refinement is given by

$$\underset{\{\mathbf{K}_L, \mathbf{K}_R, \mathbf{R}, \mathbf{t}\}}{\operatorname{argmin}} \sum_i \epsilon_i^2, \tag{10}$$

where the camera parameters $\mathbf{K}_L$, $\mathbf{K}_R$, $\mathbf{R}$ and $\mathbf{t}$ computed by the embedded calibration described in section II are corrected. We correct the extrinsic parameters as well as the focal lengths of the stereo cameras, and leave the aspect ratios, principal point positions and skew coefficients to be fixed assuming that the error introduced with this approximation is normally well-within the radius of convergence of the non-linear optimization. Equation (10) can be solved via the LM method.

IV. EXPERIMENTAL RESULTS

In this section, we provide several experiments to verify the effectiveness and accuracy of our calibration technique. The stereo head comprises two FFMV-03MTC Color Cameras (Point Gray Inc.) with TAMRON-TV varifocal lens. The calibration device is placed about 0.8 meters away from the stereo camera and a box is placed about 5 meters away. We mark four points which are the vertexes of the box, as shown in Fig. 4(a). The four points form three lines which are not totally perpendicular to each other.

Fig. 4 shows the epipolar geometry estimated by the conventional calibration method, the embedded calibration method, and the proposed method. The scene features are extracted with SIFT [23] from the images of the left and right cameras, and are matched by using a fast nearest-neighbor algorithm. The normalized 8-point algorithm [26] is implemented in a RANSAC [24] procedure to eliminate the outliers, i.e. the false-matched point pairs. Fig. 4(c) is the epipolar geometry estimated with the embedded calibration method. It is obvious that the points do not lie on the epipolar lines. The proposed method optimizes the embedded calibration with those scene features, and obtains good results as shown in Fig. 4(d). We can see the results of the proposed

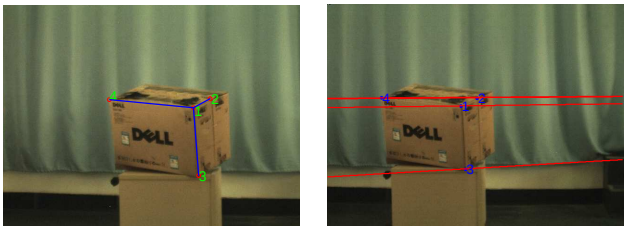

(a) The points (b) Conventional calibration

(c) Embedded calibration (d) Calibration with scene features

Fig. 4. The epipolar geometry estimated with different calibration methods.

TABLE I

THE ANGLE OF THE CORNERS (°).

	2-1-3	3-1-4	2-1-4
Conventional calibration	92.81	96.52	110.14
Embedded calibration	95.40	92.43	145.52
Proposed method	94.43	95.17	118.99

method is similar to the epipolar geometry estimated with the conventional calibration method (Fig. 4(b)).

The four vertexes and the three lines (labeled in Fig. 4(a)) are respectively reconstructed by the three methods above. The angle of the corners are computed and shown in Table I. In this experiment, the camera parameters estimated by the conventional method is regarded as the ground truth.

For quantitative comparison, one point (x, y) in the left image is mapped to 3D Euclidean coordinate (X, Y, Z) related to the left camera frame (reference camera frame) using the geometry and the disparity-depth relationship. The transformation can be described as

$$Z = \frac{Bf}{d}, X = \frac{Z(x - u_0)}{f}, Y = \frac{Z(y - v_0)}{f} \qquad (11)$$

where d denotes the disparity value, B represents the stereo baseline, and f is the focal length of the left camera. The disparity value d could be computed from the rectified images. The parameters such as (u_0, v_0), B and f are acquired from calibration results.

A planer pattern with many precise grids is designed for accuracy evaluation since the precise ground truth of the depth value (the variable Z in (11)) might be difficult to obtain. As shown in Fig. 5, we label six points on the planer pattern and indicate them by the red dots and numbers. Five lines and five angles that formed by the six points are chosen for accuracy evaluation. The planer pattern is placed at fifteen different positions. The comparative results are shown in Table II and Table III, we can see that the results of our method are comparable with the results of the

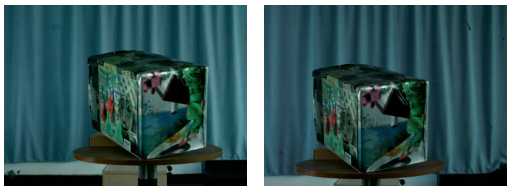

Fig. 5. The stereo pair of a box which is covered with color patterns.

conventional calibration. The embedded calibration method is not evaluated in the quantitative experiments since the epipolar geometry estimated by the embedded calibration method is not good (see Fig. 4(c)).

At last, we recover the dense depth map of a box at the distance of about 3.5 meters away from the camera. The box is covered with some color images from the data sets "Cones" and "Teddy" [13]. The stereo matching problem is formulated by Markov Random Fieds (MRF) and solved with Graph-cuts [25]. Fig. 6 shows the stereo image pair of the box. Since the region of interest is only the box, we employ a simple method to subtract the background (the blue curtains and the wall) and the useless regions (the desk). The dense depth maps are shown in Fig. 7. As can be seen, the proposed method has similar results with the conventional method.

V. CONCLUSION AND DISCUSSION

This paper has presented a new stereo camera calibration technique with an embedded calibration device and scene features. An embedded calibration method is carried out with the embedded calibration device on our stereovision system which consists of a stereo head, a half-mirror, a light source, and the calibration device. In this stereovision system, the cameras could be strongly calibrated. The scene features are used to refine the embedded calibration so that the calibration is valid for the region in the scene. Thus, the proposed method can calibrate the cameras automatically without considering variation of camera parameters.

VI. ACKNOWLEDGMENTS

This work was supported in part by the 973 Program of China under Grant No. 2012CB720000 and Natural Science Foundation of China (NSFC) under Grant No. 90920009.

(a) Conventional calibration (b) Embedded calibration (c) Calibration with scene features

Fig. 6. Depth map recovery after background subtraction. In the depth map, the closer the objects to the camera are, the higher the intensity level is.

TABLE II

THE LENGTH OF THE LINES LABELED IN FIGURE 5.

		1-2	2-3	3-4	3-5	5-6
Ground truth(mm)		200	160	40	120	80
Conventional	Length(mm)	200.91	161.04	40.42	120.88	81.37
	Mean error(%)	0.86	0.34	0.75	1.17	0.56
Proposed Method	Length(mm)	201.26	163.84	41.15	121.25	81.80
	Mean error(%)	3.27	2.76	2.98	3.25	2.49

TABLE III

COMPARATIVE RESULTS FOR ANGLES CHOSEN FROM THE PLANER PATTERN.

		1-2-3	2-3-5	4-3-5	2-4-6	2-1-6
Ground truth(°)		90	90	90	45	45
Conventional	Degree(°)	89.88	90.09	90.15	45.13	44.78
	Mean error(%)	0.48	0.50	1.07	0.75	0.68
Proposed Method	Degree(°)	89.83	90.11	89.97	44.49	45.60
	Mean error(%)	2.53	2.42	2.39	2.41	3.75

REFERENCES

[1] Olivier Faugeras, Giorgio Toscani, "The calibration problem for stereo", *In Proceedings of the International Conference on Computer Vision and Pattern Recognition*, 1986, pp. 15-20.

[2] R.Y. Tsai, "An Efficient and Accurate Camera Calibration Technique for 3D Machine Vision", *In Proceedings of the International Conference on ComputerVision and Pattern Recognition*, 1986, pp. 364-374.

[3] Y. Katayama, "Camera Calibration with a Transparent Calibration Tool Using Color Filters: Application to Stereo Camera Calibration for a Distant Object", *In Eighteenth International Conference on Pattern Recognition*, 2006, pp. 607-612.

[4] S. Bougnoux, "From projective to Euclidean space under any practical situation, a criticism of self-calibration", *In Sixth International Conference on Computer Vision*, 1998, pp. 790-796.

[5] L. Zhang and B. Li and Y. Jia, "A practical calibration method for multiple cameras", *International Conference on Image and Graphics*, 2007, pp. 45-50.

[6] P. Sturm and S. Maybank, "On plane-based camera calibration: A general algorithm, singularities,applications", *IEEE Conference on Computer Vision and Pattern Recognition*, 1999, pp. 432-437.

[7] Z. Zhang, "Camera calibration with one-dimensional objects", *European Conference on Computer Vision*, 2002, pp. 161-174.

[8] Z. Zhang, "Motion of a stereo rig: Strong, weak and self calibration", *Asian Conference on Computer Vision*, 1995, pp. I274-281.

[9] T. Ueshiba and F. Tomita, "Plane-based calibration algorithm for multi-camera systems via factorization of homography matrices", *International Conference on Computer Vision*, 2003, pp. 966-973.

[10] L. Wang and F. C. Wu and Z.Y. Hu, "Multi-camera calibration with onedimensional object under general motions", *International Conference on Computer Vision*, 2007, pp. 1-7.

[11] P. Hammarstedt and P. Sturm and A. Heyden, "Degenerate cases and closed-form solutions for camera calibration with one-dimensional objects", *International Conference on Computer Vision*, 2005, pp. 317C324.

[12] P.R.S. Mendonca and R. Cipolla, "A simple technique for self-calibration", *IEEE Conference on Computer Vision and Pattern Recognition*, 2005, pp. 317C324.

[13] D. Scharstein and R. Szeliski, "High-accuracy stereo depth maps using structured light", *IEEE Conference on Computer Vision and Pattern Recognition*, 2003, pp. 195-202.

[14] Yunde Jia and Xiameng Qin, "An embedded calibration stereovision system", *IEEE Conference on Intelligent Vehicles Symposium (IV)*, 2012, pp. 1072 -1077.

[15] J. Weng, P. Cohen, M. Herniou, Camera calibration with distortion models and accuracy evaluation, *IEEE Transactions on Pattern Analysis and Machine Intelligence*, vol. 14, 1992, pp 965-980.

[16] Zhang Zhengyou, A flexible new technique for camera calibration, *IEEE Transactions on Pattern Analysis and Machine Intelligence*, vol. 20, 2000, pp 1330-1334.

[17] Zhengyou Zhang, A stereovision system for a planetary rover: calibration, correlation, registration, and fusion, *Machine Vision and Applications*, vol. 10, 1997, pp 27-34.

[18] Zhengyou Zhang, Determining the Epipolar Geometry and Its Uncertainty: A Review, *International Journal of Computer Vision*, vol. 27, 1998, pp 161-195.

[19] I. Miyagawa and H. Arai and H. Koike, Simple camera calibration from a single image using five points on two orthogonal 1-d objects, *IEEE Transactions on Image Processing*, vol. 19, 2010, pp 1528-1538.

[20] T. Dang and C. Hoffmann and C. Stiller, Continuous Stereo Self-Calibration by Camera Parameter Tracking, *IEEE Transactions on Image Processing*, vol. 18, 2009, pp 1536-1550.

[21] S. J. Maybank and O. D. Faugeras, A theory of self-calibration of a moving camera, *International Journal of Computer Vision*, vol. 8, 1992, pp 123-151.

[22] F. C. Wu and Z. Y. Hu and H. J. Zhu, Camera calibration with moving one-dimensional objects, *Pattern Recognition*, vol. 38, 2005, pp 755-765.

[23] David G. Lowe, Distinctive Image Features from Scale-Invariant Keypoints, *International Journal of Computer Vision*, vol. 60, 2004, pp 91-110.

[24] Fischler, M.A. and Bolles, R.C., Random sample consensus: a paradigm for model fitting with applications to image analysis and automated cartography, *Communications of the ACM*, vol. 24, 1981, pp 381-395.

[25] Y. Boykov and O. Veksler and R. Zabih, Fast approximate energy minimization via graph cuts, *IEEE Transactions on Pattern Analysis and Machine Intelligence*, vol. 23, 2001, pp 1222–1239.

[26] R. Hartley, A. Zisserman, *Multiple View Geometry in computer vision*, Cambridge University Press, 2000.

[27] J.Y. Bouguet, Camera Calibration Toolbox for Matlab, `http://www.vision.caltech.edu/bouguetj/calib_doc/`, 2004.